_____

The Impact of the Preparation Procedure on the Structural, Optical, and Magnetic Characteristics of Nickel Ferrite Nanoparticles.

Nisha Chaudhary[1] and Vikram Singh[2] *

[1]*Ph.D. Scholar (Department of Physics), Om Sterling Global University, Hissar (125001)*

[2]*Assistant Professor (Department of Physics), Om Sterling Global University, Hissar (125001)*

*Corresponding Author: Vikram Singh

 Abstract

Nanocrystalline $NiFe_2O4$ particles were synthesized using traditional sol-gel, citrate-nitrate sol-gel combustion, and coprecipitation techniques. The synthesized samples underwent annealing at a temperature of 1000 °C for two hours. Subsequently, an investigation was conducted to analyze the structural, chemical, morphological, optical, and magnetic properties of nickel ferrite. The X-ray diffraction (XRD) technique was used to analyze the structural properties, which validated the creation of single-phase $NiFe_2O_4$ particles using all three methods. The chemical characteristics were assessed using Fourier transform infrared (FT-IR) spectroscopy, which verified the presence of the correct vibration modes in the samples. The UV-Vis spectroscopy technique was used to investigate the optical characteristics. The as-synthesized materials were analyzed using scanning electron microscopy (SEM) to determine their morphology. The scanning electron microscopy (SEM) scans revealed the presence of clustered nanoparticles of NiFe2O4. The magnetic characteristics were examined using a vibrating sample magnetometer (VSM), which revealed that the calcined samples had characteristic magnetic behavior.

Keywords: NFO magnetic properties; NFO structural properties; NFO morphology

Introduction

Ferrites are the most important soft magnetic materials because of their high specific heat, low melting point, large coefficient of expansion, low magnetic phase transition temperature, and low saturated magnetic moments [1]. They are attractive for gas sensors, microwave and electronic devices, communications equipment, magnetic storage, and magnetic fluids due to their unique properties [2]. Ferrites are also used for hypothermia and inter-body drug transmission [3]. Nanosized ferrites have a spinel structure with the structural formula MFe2O4, where M is a divalent metal ion like Ni, Cu, Zn, Co, Mn, Mg, etc [4]. These compounds are useful in electronics, telecommunications, and power generation due to their magnetic characteristics [5]. Ferrites are utilized as magnetic cores in transformers, inductors, and other electronics. [6] They concentrate and direct magnetic fields while minimizing energy losses from eddy currents because of their high magnetic permeability and low electrical conductivity [7]. Power transfer and signal filtering in electronic circuits are efficient with this characteristic. Ferrites are essential to antenna and RF device design in telecommunications. They are used as ferrite beads or cores to reduce EMI and improve signal integrity. Ferrite materials may selectively absorb or reflect electromagnetic radiation within specified frequency ranges, making wireless signal transmission and receiving efficient. Ferrites are also employed in automobile ignition systems, sensors, and electric motors [8]. They produce strong and reliable magnetic fields in automobile components due to their high coercivity and magnetic stability. Ferrites enhance energy efficiency and reduce electrical equipment losses in power generating and distribution systems. Transformers, inductive heating systems, and MRI machines use them to optimize energy transfer and

_____

reduce electromagnetic interference [9]. Ferrites enable modern electronics, telecommunications, and energy infrastructure to work efficiently and reliably. Their magnetic qualities fuel innovation in electronics, communications, and sustainable energy solutions.

The magnetic and electrical properties of ferrite nanocrystals are determined by the characteristics of the ions and their charges, as well as their distribution on tetrahedral (A) and octahedral (B) sites. Among the various types of ferrites, nickel ferrite stands out as a versatile and technologically advanced soft magnetic ceramic material [10]. It possesses highly desirable qualities such as high electrical resistivity, excellent electrochemical stability, a high Curie temperature, low magnetostriction, low magnetic coercivity, low magnetic anisotropy, high permeability in the RF region, and a high Neel temperature [12]. Furthermore, nickel ferrite exhibits low eddy current loss, making it an ideal choice for power transformers.

Nickel ferrite exhibits an inverse spinel crystal structure. The structure is a face-centered cubic arrangement, with a total of 32 oxygen ions present in each unit cell. The oxygen ions are present in 64 tetrahedral and 32 octahedral positions [13]. In nickel ferrite, the A sites are occupied by ferric ions (Fe^{3+}), whereas the B sites are filled with a 1:1 combination of nickel ions (Ni^{2+}) and ferric ions (Fe^{3+}). The Ni^{2+} ions are located at the B sites and are surrounded by the O^{2-} ions in an octahedral coordination arrangement. Therefore, the chemical can be represented by the formula. The chemical formula is $Fe^{3+}A[Ni^{2+}Fe^{3+}]BO^{2-}$ The given text consists of the number 4 and a list containing the numbers 19 and 20. The ferromagnetic behavior of this ferrite is caused by the presence of magnetic moments with anti-parallel spins between Fe^{+3} ions located at tetrahedral positions and Fe^{+3} and Ni^{+2} ions at octahedral positions [14]. The distinctive behaviors of $NiFe_2O_4$ are linked to the structure and microstructural components of the nanoparticles, which are very responsive to the synthesis methods employed. Various chemical and physical techniques have been employed to create ferrite nanoparticles, such as sonochemical reactions, solid-state reactions, microwave plasma, high-temperature self-propagation, solvothermal synthesis, sol-gel methods, chemical co-precipitation, and hydrothermal method [15]. In addition, sol-gel wet chemical, sol-gel autocombustion, and co-precipitation procedures are highly advantageous. The standard sol-gel approach is advantageous due to its ability to achieve a tiny particle size, excellent homogeneity, facile shape and doping, good stoichiometric control, and improved phase purity compared to conventional ceramic procedures [16]. The sol-gel auto-combustion method is advantageous since it utilizes inexpensive precursors and allows for a straightforward synthesis process, resulting in the production of a fine and uniform powder [17]. On the other hand, the co-precipitation method is employed due to its benefits, such as operating at low temperatures, allowing for precise control of average grain size by regulation of the precipitation reaction, and achieving a high output rate [18]. The synthesis of $NiFe_2O_4$ nanoparticles was carried out using three different methods: conventional sol-gel (CSG), citrate-nitrate sol-gel combustion (SGC), and co-precipitation (Co-P). An analysis was conducted on the microstructures and magnetic characteristics of the sintered CSG, SGC, and Co-P generated samples, and a detailed comparison is provided.

Experimental

Figure 1 displays the schematic flowchart outlining several experimental protocols employed in the production of $NiFe_2O_4$ Nanopowders. The initial substances used in all three methods were iron nitrate [$(Fe(NO_3)_3 \cdot 9H_2O)$]. and a compound called nickel nitrate.

The chemical compound is represented by the formula [$(Ni(NO_3)_2 \cdot 6H_2O)$]. The chemicals used were of analytical quality and had a purity level of 99.99%. They were utilized as received without undergoing any additional purification processes. In the CSG approach, metal salts were dissolved individually in ethylene glycol with the assistance of magnetic stirring [19].

The two solutions were thereafter combined and maintained under continuous agitation for one hour. The resulting clear solution was subjected to heating in an electric oven at a temperature of 80 °C to generate a wet gel. The gel was dehydrated at a temperature of 120 °C in the same oven for 12 hours. Spontaneous combustion occurred, resulting in a large and fluffy product with a brown color [1, 20]. The powder acquired by this method was finely pulverized and subjected to annealing at a temperature of 1000 °C for two hours in an electric furnace.

_____

Citric acid monohydrate was employed in SGC as both a chelating agent and a fuel for the combustion process. Deionized water was utilized to dissolve the initial metal salts, with a molar ratio of citrate/nitrate (C/N) of 1. The pH of the solution was approximately neutralized to 7 by introducing a small quantity of ammonia. Throughout this procedure, the solution was consistently stirred using a magnetic bar agitator. The resultant solution was heated with agitation at a temperature of 85 °C to remove the surplus solvent and create a gel. The gel was transferred to a bowl and heated on a hot plate at a temperature of 120 °C. When the temperature reached 300 °C, the dried gel ignited and burned in a self-sustaining manner until the entire gel was entirely consumed, resulting in the formation of a loose powder. The powder underwent annealing at a temperature of 1000 °C for two hours to achieve the final product. In the Co-P method, the exact amount of metal salt required was dissolved in a suitable quantity of deionized water [20]. The prepared solutions were combined using a micropipette while being continuously stirred. The pH of the solution was precisely controlled by adding sodium hydroxide (NaOH) solution, which served as a precipitating agent. Thus, the formation of brown-colored precipitates occurred in this manner [21]. The sodium hydroxide, along with any other contaminants, was eliminated through the process of filtration and repeated washing of the precipitates with deionized water. The precipitate was subjected to a drying process in an electric oven at a temperature of 150 °C for two hours. The obtained product underwent milling and was subsequently annealed for two hours at a temperature of 1000 °C to obtain the final fine nickel ferrite ($NiFe_2O_4$) nanoparticles.

Characterization

The structural analysis of the annealed powders of the samples was conducted using an X-ray diffractometer (Rigaku DMAX-3A) equipped with $CuK\alpha$ radiation (wavelength of 1.5406 A). To analyze the microstructure of the calcined materials, we used a JEOL JSM-6510LV scanning electron microscope (SEM) to capture scanned micrographs [22]. The Fourier transform infrared spectra were obtained using a Perkin-Elmer 100 Series FT-IR spectrometer, with potassium bromide (KBr) serving as the solvent. The optical characterisation was conducted using a Perkin-Elmer, LAMBDA 950 UV-Vis-NIR spectrometer. The magnetic characteristics of the finished powders were examined using a vibrating sample magnetometer (VSM) to measure the magnetic hysteresis loops [23].

Results and discussion

Figure 1, 2 and 3 displays the X-ray diffraction (XRD) patterns of $NiFe_2O_4$ powder samples that were synthesized using the Co-P techniques, SGC and CGS. The distinct peaks observed in the diffractograms indicate the presence of a completely crystalline phase of nickel ferrite ($NiFe_2O_4$) with a clearly defined cubic spinel crystal structure [24]. The primary peak is located at $2\theta = 34.5°$ and corresponds to the crystal plane with Miller indices (310), which is specific to the $NiFe_2O_4$ cubic spinel. The distinct peaks observed in the XRD patterns. Upon analyzing the XRD pattern, the peak locations and relative intensities were used to determine that the powder samples synthesized and calcined at 1000 °C are cubic spinel nickel ferrite ($NiFe_2O_4$). Nevertheless, a small number of impurity peaks were detected in the sample obtained through auto-combustion. These peaks correspond to the presence of the hematite phase (α-Fe_2O_3) [25]. The average diameters of the crystallite particles were determined for all the samples by utilizing the Debye-Scherrer equation and the high-intensity peak (310).

$$D = \frac{k\lambda}{\beta \cos\theta}$$

The variables in the equation are as follows: D represents the average particle size, k is the particle shape factor with a value of 0.87, λ represents the wavelength of the X-ray beam employed with a value of 0.156 nm, β is the full width at half-maximum (FWHM) of the (3 1 1) plane, and θ represents Bragg's angle [26].. The equation was used to determine the average lattice constant a for the (310) plane.

_____

$$a = \frac{\sqrt{h^2 + k^2 + l^2}}{2\sin\theta}$$

The average X-ray density of the nickel ferrite nanoparticles was determined using the relation

$$\rho_x = 8M/Na^3$$

where M is the molecular weight (for nickel ferrite: 234.3816 g·mol−1), N is Avogadro's number (6.02 × 1023 mol−1) and a is the lattice constant.

Figure 4,5 and 6 displays the FT-IR spectra of the examined NiFe2O4 samples, which provide evidence for the creation of the spinel structure. Within the infrared region, two primary frequency modes are detected, spanning from 1100 cm−1 to 400 cm−1. The higher band (v1), typically found between 500 cm−1 and 540 cm−1, is associated with the stretching frequency of the tetrahedral metal-oxygen bond [27]. The lowest band (v2), commonly observed between 430 cm−1 and 371 cm−1, is attributed to the vibration mode of the octahedral metal-oxygen bond [28]. Their values align precisely with the values documented in the literature [29, 30]. The spectra also exhibit prominent bands at around 3452 cm−1 and 1530 cm−1, which are attributed to the vibrational modes of H–O stretching and bending in free or absorbed water. The band observed at a frequency of 1120 cm−1 is a result of the anti-symmetric stretching vibrations of NO molecules, indicating the presence of nitrates in the samples [31]. Figure 7 displays the UV-Vis absorption spectra of $NiFe_2O_4$ nanocrystals obtained using sol-gel, auto-combustion, and co-precipitation methods, with the spectra varying according to the wavelength. The determination of the band gap energy was performed via Tauc's scheme. Tauck's equation [32, 33] states that the absorption coefficient near the band edge is determined for a direct bandgap material.

$$\alpha = \frac{A}{h\upsilon}(h\upsilon - E_g)^{\frac{1}{2}}$$

The variables in the equation are defined as follows: α represents the absorption coefficient, hυ represents the photon energy, Eg represents the band gap energy, and A is a constant that varies depending on the kind of transition.

Equation indicates that when the product of αhυ is equal to zero, the value of Eg is equal to hυ. The band gap energy can be found by charting the square of the product of the absorption coefficient (α) and the photon energy (hυ) against the photon energy (hυ), and then extrapolating the plot to locate the intercept on the photon energy axis where the square of the product of the absorption coefficient and the photon energy is equal to zero [34]. The band gap energy has been calculated by identifying the point where the straight line intersects with = 0 for all samples. The band gap of the samples falls within the range of 5.2 eV to 5.9 eV, which is similar to the values reported in [35]. The UV-Vis spectra of all samples unambiguously demonstrate the ability of NiFe2O4 nanocrystals to efficiently absorb energy in the given range. The wavelength range spans from 219 nm to 230 nm.

The magnetic characteristics of NiFe2O4 nanoparticles were examined using a vibrating sample magnetometer (VSM) at normal room temperature. Figure 8, 9, 10 displays the hysteresis loops of NiFe2O4 nanoparticles with an imposed external magnetic field of 15 kOe The CSG generated sample exhibits the highest saturation magnetization, measuring approximately 36.61 emu/g. The magnetic saturation (Ms) values of the synthesised NiFe2O4 nanoparticles are considerably lower than the Ms values of the bulk NiFe2O4 (55 emu/g). The reduction in saturation magnetization of these samples, in comparison to that of the bulk material, is contingent upon many parameters [36]. The heating rate of the calcination process is a crucial parameter in the thermal treatment procedure, since it has a significant impact on the saturation magnetization, either increasing or decreasing it. The heating rate of calcination in this experiment was approximately 10 °C/min, which can be considered relatively high. Thus, it is plausible that employing a slower heating rate during calcination would enhance the degree of crystallization and potentially lead to an augmentation in the magnetic phase, thereby resulting in greater

_____

saturation magnetization.. SGC had a significantly low saturation magnetization of approximately 3.66 emu/g. The generated sample may also be influenced by the presence of a weakly magnetic and impure fraction of hematite. Conversely, a rise in saturation magnetization was noted as the particle size increased. The presence of slanted or distorted spins on the surface of the nanoparticles causes repulsion of the core spins, leading to alignment with the field direction. Following that, the saturation magnetization attains lower values [37, 38]. The magnetic analysis demonstrates that the traditional sol-gel technique yields nickel ferrite particles with a moderate level of magnetism and an extremely low level of hysteresis loss, as shown in.

The morphology of the synthesized NiFe2O4 samples was observed using scanning electron microscopy (SEM) to investigate the impact of the synthesis route. Figure 11 displays scanning electron microscope (SEM) pictures of NiFe2O4 powder that underwent calcination at a temperature of 1000 °C [39, 40]. The micrographs depict well-formed particles that are clustered together to create uneven formations. The agglomeration process may be attributed to magnetic attraction. However, there exists a significant abundance of crystals that possess a consistent and even range of sizes. Nevertheless, the sol-gel generated sample exhibits a significantly larger crystal size compared to the other two samples, with grain sizes ranging from approximately 0.38 µm to 2.7 µm. The results obtained are consistent with the XRD data, which show distinct peaks indicating a well-defined crystallization of $NiFe_2O_4$. This suggests that the method used for synthesis greatly influences the shape and structure of the particles.

Conclusions

We have successfully produced nickel ferrite nanoparticles using sol-gel wet chemical, sol-gel auto-combustion, and co-precipitation techniques. The XRD data verified the crystalline nature of the particles. The sample obtained from the sol-gel process exhibited greater purity in comparison to the other two samples. The magnetic analysis clearly demonstrated that the sol-gel technique yielded nanoparticles with a reasonable level of magnetization and a low degree of hysteresis loss. The lower magnetic susceptibility (MS) value seen in the prepared samples can be related to the higher proportion of surface spins in these nanoparticles. These surface spins tend to be in a canted, spin-glass-like-ordered phase, resembling a state with a reduced magnetic moment. The sol-gel wet chemical approach is the optimal choice for synthesizing pure crystalline nickel ferrite nanoparticles due to its high level of crystallinity, mild magnetism, and minimal hysteresis loss. This process, which is both easy and cost-effective, can also be used to synthesize additional spinel ferrite nanoparticles that are of interest in the field of nanotechnology. Additionally, this method is environmentally friendly.

References

1. Lenin, N., Sakthipandi, K., Kanna, R. R., & Rajesh, J. (2018). Effect of neodymium ion on the structural, electrical and magnetic properties of nanocrystalline nickel ferrites. *Ceramics International*, *44*(10), 11562-11569.
2. Hajalilou, A., & Mazlan, S. A. (2016). A review on preparation techniques for synthesis of nanocrystalline soft magnetic ferrites and investigation on the effects of microstructure features on magnetic properties. *Applied Physics A*, *122*, 1-15.
3. Hajalilou, A., & Mazlan, S. A. (2016). A review on preparation techniques for synthesis of nanocrystalline soft magnetic ferrites and investigation on the effects of microstructure features on magnetic properties. *Applied Physics A*, *122*, 1-15.
4. Nandapure, A. I., Kondawar, S. B., Sawadh, P. S., & Nandapure, B. I. (2012). Effect of zinc substitution on magnetic and electrical properties of nanocrystalline nickel ferrite synthesized by refluxing method. *Physica B: Condensed Matter*, *407*(7), 1104-1107.
5. Hajalilou, A., Hashim, M., Ebrahimi-Kahrizsangi, R., & Kamari, H. M. (2015). Influence of evolving microstructure on electrical and magnetic characteristics in mechanically synthesized polycrystalline Ni-ferrite nanoparticles. *Journal of Alloys and Compounds*, *633*, 306-316.
6. Patange, S. M., Shirsath, S. E., Toksha, B. G., Jadhav, S. S., & Jadhav, K. M. (2009). Electrical and magnetic properties of Cr3+ substituted nanocrystalline nickel ferrite. *Journal of applied physics*, *106*(2).

_____

7. Adam, A., Ali, Z., Abdeltwab, E., & Abbas, Y. (2009). Magnetic and structural investigations of nanocrystalline nickel ferrite NiFe2O4. *Journal of Ovonic Research Vol*, *5*(5), 157-165.

8. Ghosh, P., Bhowmik, R. N., Das, M. R., & Mitra, P. (2017). Electrical conductivity and magnetic field dependent current-voltage characteristics of nanocrystalline nickel ferrite. *Physica E: Low-dimensional Systems and Nanostructures*, *88*, 218-227.

9. Nasir, S., Asghar, G., Malik, M. A., & Anis-ur-Rehman, M. (2011). Structural, dielectric and electrical properties of zinc doped nickel nanoferrites prepared by simplified sol–gel method. *Journal of sol-gel science and technology*, *59*, 111-116.

10. Kumari, M., & Bhatnagar, M. C. (2019). Study of the effect of Pr doping on structural, morphological and magnetic properties of nickel ferrite. *Journal of Superconductivity and Novel Magnetism*, *32*, 1027-1033.

11. Kumar, E. R., Kamzin, A. S., & Prakash, T. (2015). Effect of particle size on structural, magnetic and dielectric properties of manganese substituted nickel ferrite nanoparticles. *Journal of Magnetism and Magnetic Materials*, *378*, 389-396.

12. Prasad, B. V., Ramesh, K. V., & Srinivas, A. (2018). Structural and magnetic properties of nanocrystalline nickel ferrite (NiFe2O4) synthesized in sol-gel and combustion routes. *Solid State Sciences*, *86*, 86-97.

13. Anu, K., & Hemalatha, J. J. C. I. (2022). Synthesis and analysis of structural, compositional, morphological, magnetic, electrical and surface charge properties of Zn-doped nickel ferrite nanoparticles. *Ceramics International*, *48*(3), 3417-3425.

14. Deraz, N. M. (2012). Effects of magnesia addition on structural, morphological and magnetic properties of nano-crystalline nickel ferrite system. *Ceramics International*, *38*(1), 511-516.

15. Ahmad, U., Afzia, M., Shah, F., Ismail, B., Rahim, A., & Khan, R. A. (2022). Improved magnetic and electrical properties of transition metal doped nickel spinel ferrite nanoparticles for prospective applications. *Materials Science in Semiconductor Processing*, *148*, 106830.

16. Akbar Hoseini, S., & Khademolhoseini, S. (2016). Investigation of the structural, optical and magnetic properties of nickel ferrite nanoparticles synthesized through modified sol–gel method. *Journal of Materials Science: Materials in Electronics*, *27*, 5943-5947.

17. Akbar Hoseini, S., & Khademolhoseini, S. (2016). Investigation of the structural, optical and magnetic properties of nickel ferrite nanoparticles synthesized through modified sol–gel method. *Journal of Materials Science: Materials in Electronics*, *27*, 5943-5947.

18. Shahbaz Tehrani, F., Daadmehr, V., Rezakhani, A. T., Hosseini Akbarnejad, R., & Gholipour, S. (2012). Structural, magnetic, and optical properties of zinc-and copper-substituted nickel ferrite nanocrystals. *Journal of superconductivity and novel magnetism*, *25*, 2443-2455.

19. Sonia, M. M. L., Anand, S., Vinosel, V. M., Asisi Janifer, M., & Pauline, S. (2018). Effect of lattice strain on structural, magnetic and dielectric properties of sol–gel synthesized nanocrystalline Ce 3+ substituted nickel ferrite. *Journal of Materials Science: Materials in Electronics*, *29*, 15006-15021.

20. Sharma, S., Verma, K., Chaubey, U., Singh, V., & Mehta, B. R. (2010). Influence of Zn substitution on structural, microstructural and dielectric properties of nanocrystalline nickel ferrites. *Materials Science and Engineering: B*, *167*(3), 187-192.

21. Sethi, N., Bhardwaj, P., Kumar, S., & Dilbaghi, N. (2019). Development and Evaluation of Ursolic Acid Co-Delivered Tamoxifen Loaded Dammar Gum Nanoparticles to Combat Cancer. *Advanced Science, Engineering and Medicine*, *11*(11), 1115-1124.

22. Sethi, N., Bhardwaj, P., Kumar, S., & Dilbaghi, N. (2019). Development And Evaluation Of Ursolic Acid Loaded Eudragit-E Nanocarrier For Cancer Therapy. *International Journal of Pharmaceutical Research (09752366)*, *11*(2).

23. Rani, P., & Sethi, N. (2024). To Combat Cancer Cell Lines, the Development, and Evaluation of Lycopene-Co-Loaded Tamoxifen Nanoparticles. Naturalista Campano, 28(1), 1158-1166.

24. Saini, A., Budania, L. S., Berwal, A., & Sethi, S. K. N. (2023). Screening of the Anticancer Potential of Lycopene-Loaded Nanoliposomes. *Tuijin Jishu/Journal of Propulsion Technology*, *44*(4), 1372-1383.

_____

25. Nabiyouni, G., Fesharaki, M. J., Mozafari, M., & Amighian, J. (2010). Characterization and magnetic properties of nickel ferrite nanoparticles prepared by ball milling technique. *Chinese Physics Letters*, *27*(12), 126401.

26. Gabal, M. A., Al-Thabaiti, S. A., El-Mossalamy, E. H., & Mokhtar, M. (2010). Structural, magnetic and electrical properties of Ga-substituted NiCuZn nanocrystalline ferrite. *Ceramics International*, *36*(4), 1339-1346.

27. Mallapur, M. M., Shaikh, P. A., Kambale, R. C., Jamadar, H. V., Mahamuni, P. U., & Chougule, B. K. (2009). Structural and electrical properties of nanocrystalline cobalt substituted nickel zinc ferrite. *Journal of alloys and compounds*, *479*(1-2), 797-802.

28. Saleem, A., Zhang, Y., Gong, H., Majeed, M. K., Jing, J., Lin, X., ... & Ashfaq, M. Z. (2020). Structural, magnetic and dielectric properties of nano-crystalline spinel NixCu1-xFe2O4. *Journal of Alloys and Compounds*, *825*, 154017.

29. Jalaiah, K., & Babu, K. V. (2017). Structural, magnetic and electrical properties of nickel doped Mn-Zn spinel ferrite synthesized by sol-gel method. *Journal of Magnetism and Magnetic Materials*, *423*, 275-280.

30. Balavijayalakshmi, J., Suriyanarayanan, N., & Jayaprakash, R. (2015). Role of copper on structural, magnetic and dielectric properties of nickel ferrite nano particles. *Journal of Magnetism and Magnetic Materials*, *385*, 302-307.

31. Yadav, R. S., Kuřitka, I., Vilcakova, J., Havlica, J., Masilko, J., Kalina, L., ... & Hajdúchová, M. (2017). Structural, magnetic, dielectric, and electrical properties of NiFe2O4 spinel ferrite nanoparticles prepared by honey-mediated sol-gel combustion. *Journal of Physics and Chemistry of Solids*, *107*, 150-161.

32. Paswan, S. K., Kumari, S., Kar, M., Singh, A., Pathak, H., Borah, J. P., & Kumar, L. (2021). Optimization of structure-property relationships in nickel ferrite nanoparticles annealed at different temperature. *Journal of Physics and Chemistry of Solids*, *151*, 109928.

33. Batoo, K. M., Kumar, S., & Lee, C. G. (2009). Finite size effect and influence of temperature on electrical properties of nanocrystalline Ni–Cd ferrites. *Current Applied Physics*, *9*(5), 1072-1078.

34. Annie Vinosha, P., Deepapriya, S., Rodney, J. D., Krishnan, S., & Jerome Das, S. (2019). Investigation on elastic, magnetic, optical and electrical impedance properties of dysprosium doped nickel ferrite nanocrystals. *Journal of Nanoscience and Nanotechnology*, *19*(12), 8020-8035.

35. Nawale, A. B., Kanhe, N. S., Patil, K. R., Bhoraskar, S. V., Mathe, V. L., & Das, A. K. (2011). Magnetic properties of thermal plasma synthesized nanocrystalline nickel ferrite (NiFe2O4). *Journal of Alloys and Compounds*, *509*(12), 4404-4413.

36. Chavan, A. R., Birajdar, S. D., Chilwar, R. R., & Jadhav, K. M. (2018). Structural, morphological, optical, magnetic and electrical properties of Al3+ substituted nickel ferrite thin films. *Journal of Alloys and Compounds*, *735*, 2287-2297.

37. Wahba, A. M., & Mohamed, M. B. (2014). Structural, magnetic, and dielectric properties of nanocrystalline Cr-substituted Co0. 8Ni0. 2Fe2O4 ferrite. *Ceramics International*, *40*(4), 6127-6135.

38. Gabal, M. A., Al Angari, Y. M., & Zaki, H. M. (2014). Structural, magnetic and electrical characterization of Mg–Ni nano-crystalline ferrites prepared through egg-white precursor. *Journal of magnetism and magnetic materials*, *363*, 6-12.

39. Bushkova, V. S., & Yaremiy, I. P. (2018). Magnetic, electric, mechanical, and optical properties of NiCrxFe2− xO4 ferrites. *Journal of Magnetism and Magnetic Materials*, *461*, 37-47.

40. Heiba, Z. K., Mohamed, M. B., Ahmed, M. A., Moussa, M. A. A., & Hamdeh, H. H. (2014). Cation distribution and dielectric properties of nanocrystalline gallium substituted nickel ferrite. *Journal of alloys and compounds*, *586*, 773-781.
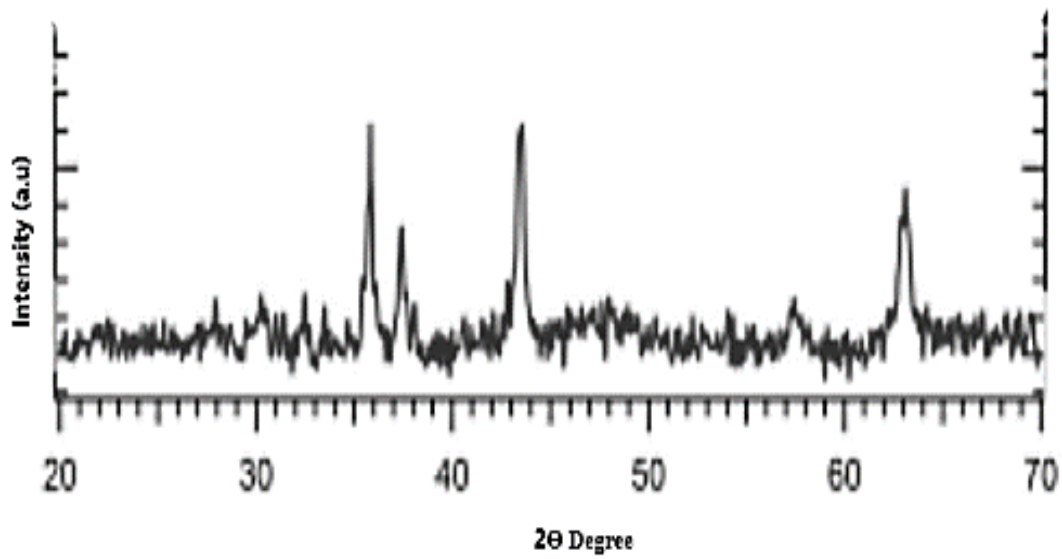
_____

Figure 1: XRD patterns of NiFe2O4 nanoparticles synthesized by Co-Precipitation method
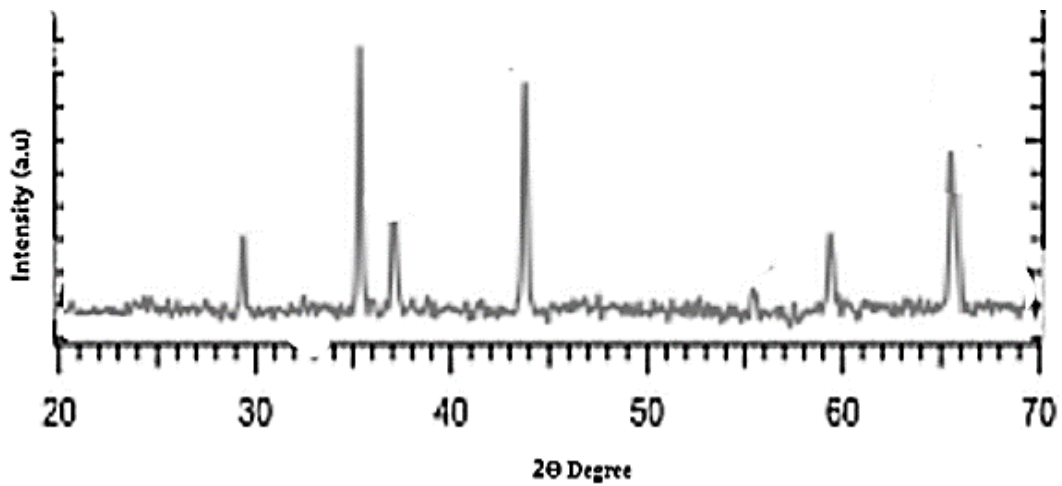

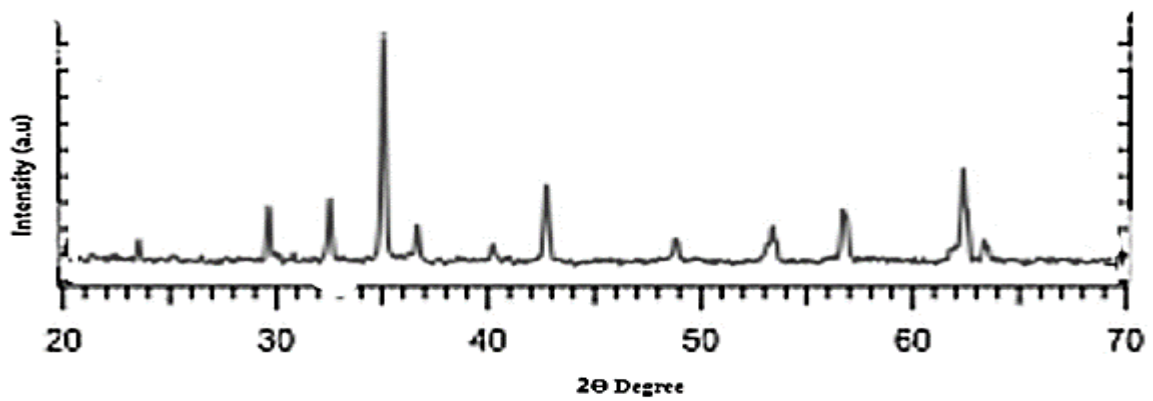**Figure 2: XRD patterns of NiFe2O4 nanoparticles synthesized by sol-gel method**

Figure 3: XRD patterns of NiFe2O4 nanoparticles synthesized by citrate-nitrate sol-gel method
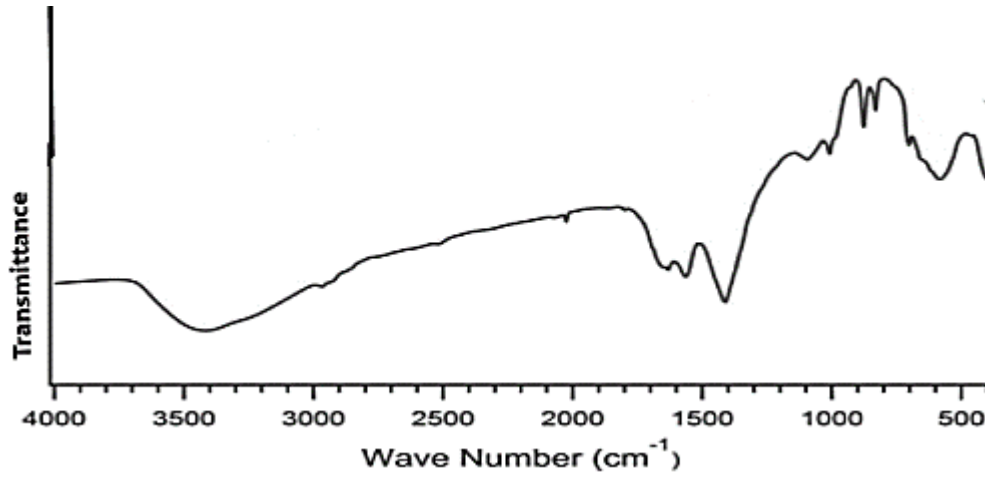
_____

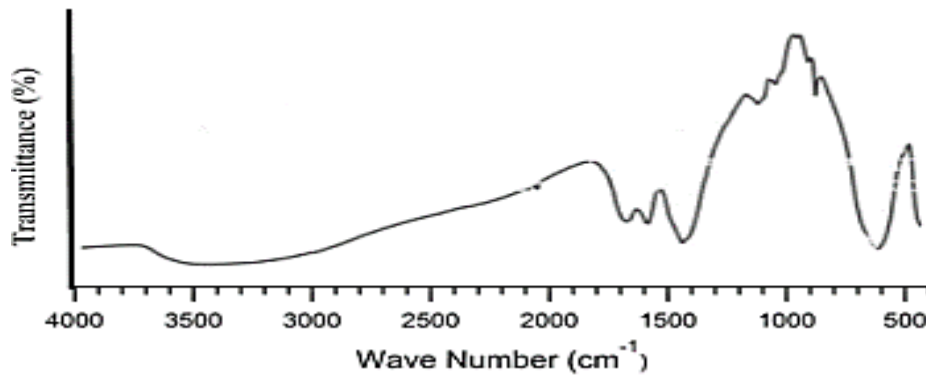**Figure 4: FT-IR spectra of NiFe2O4 nanoparticles synthesized by Co-P methods**

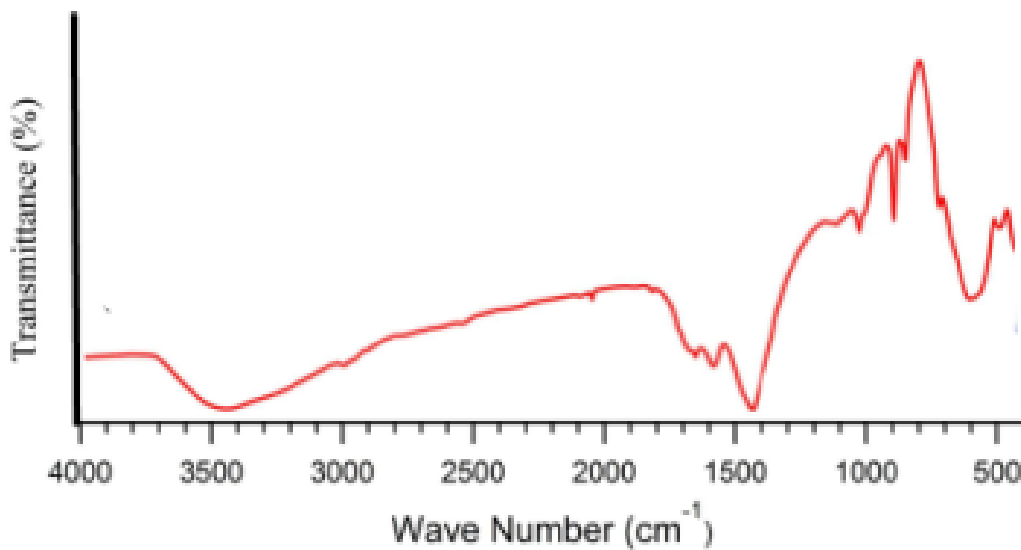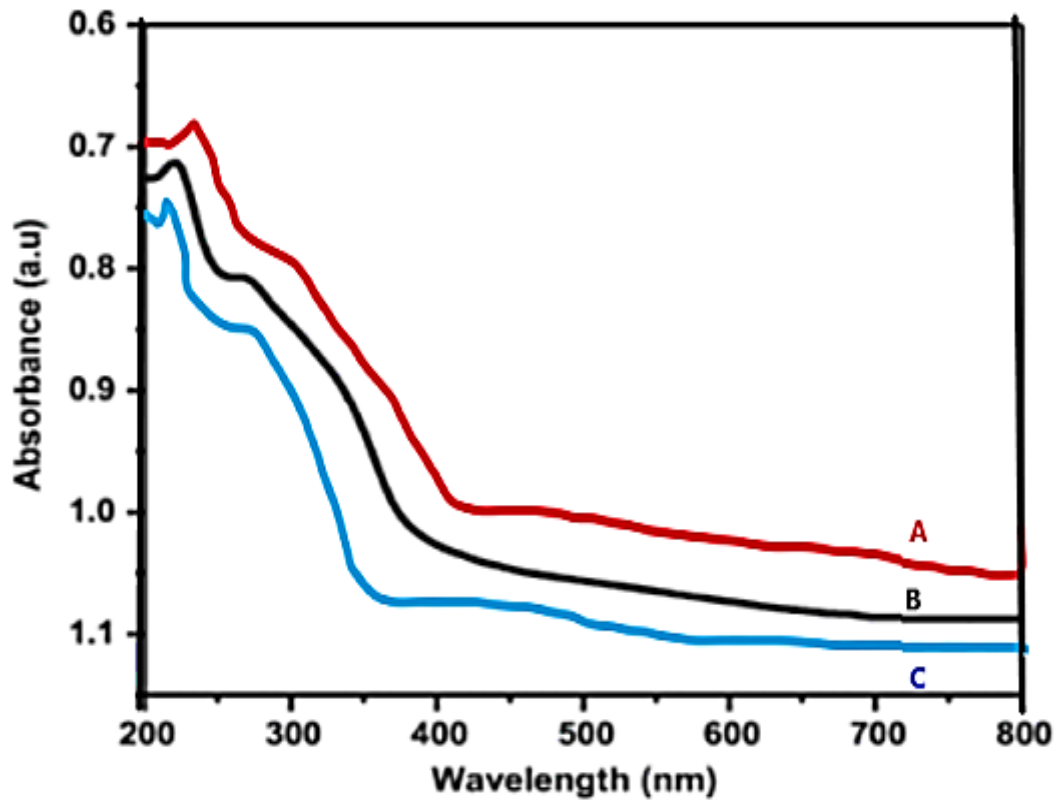**Figure 5: FT-IR spectra of NiFe2O4 nanoparticles synthesized by citrate nitrate sol-gel methods**

Figure 6: FT-IR spectra of NiFe2O4 nanoparticles synthesized by conventional sol-gel methods

_____

Figure 7: UV spectra of NiFe2O4 nanoparticles synthesized by A) Co-precipitation method B) Citrate nitrate sol gel method C) Conventional sol-gel methods
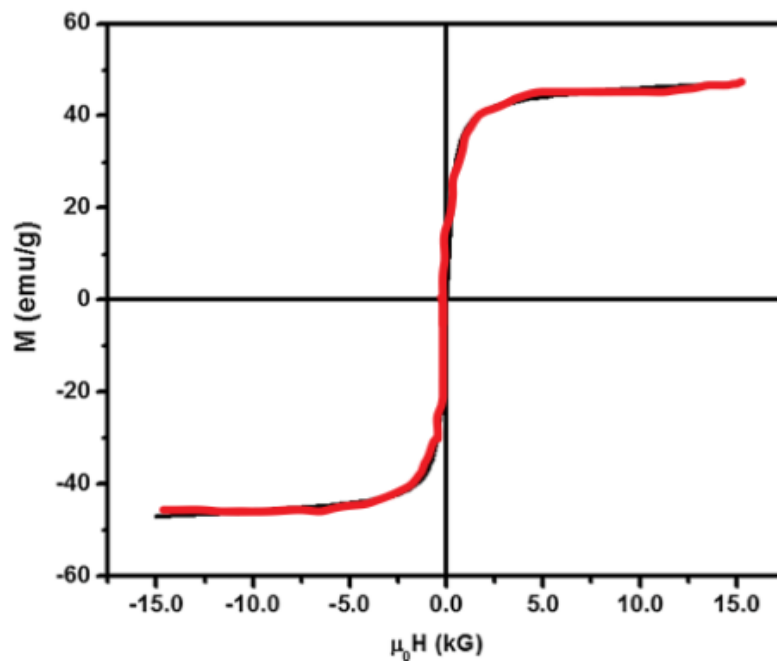

Figure 8: Magnetic hysteresis curves of samples NiFe$_2$O$_{4-3}$ by Co-precipitation method
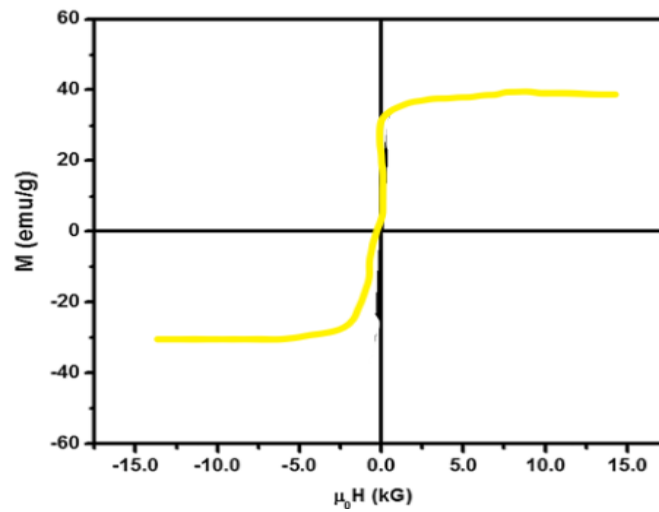
Figure 9: Magnetic hysteresis curves of samples NiFe$_2$O$_{4-3}$ by Citrate nitrate sol-gel method
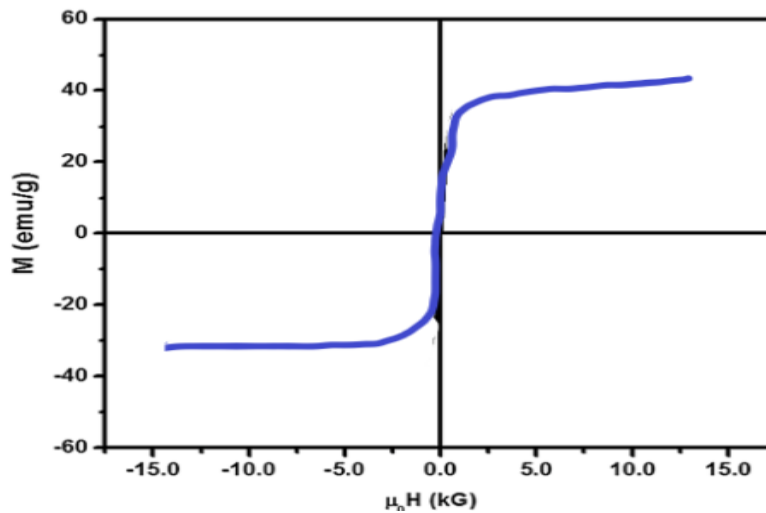

Figure 10: Magnetic hysteresis curves of samples NiFe$_2$O$_{4-3}$ by Conventional sol-gel methods
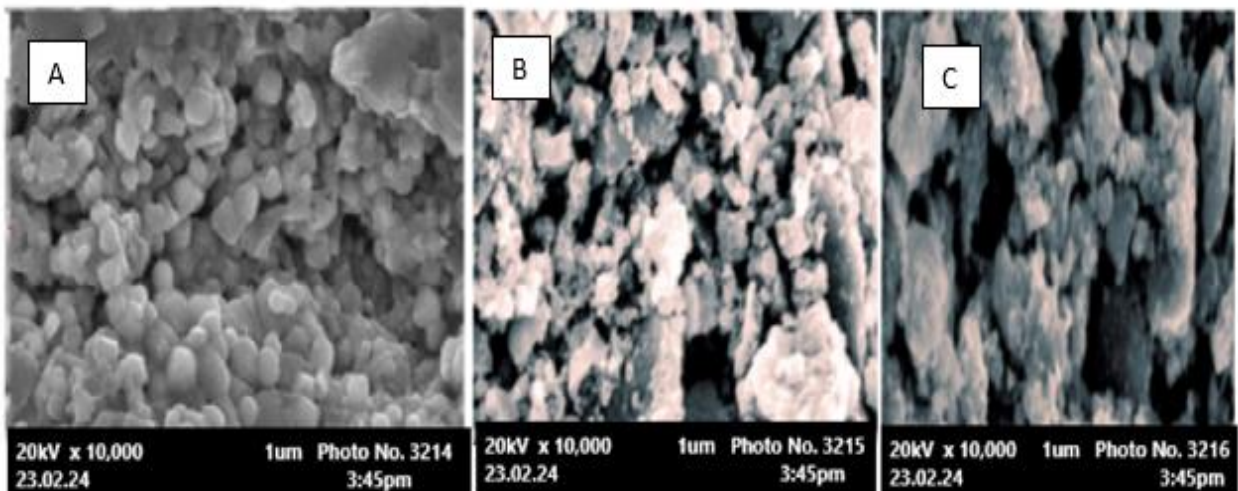

Figure 11: SEM Image of A) Co-precipitation method B) Citrate nitrate sol-gel method C) Conventional sol-gel methods at 1000°C